Plasmons in graphite and stage-1 graphite intercalation compounds

M. F. Lin, C. S. Huang, and D. S. Chuu
Electrophysics Department, National Chiao Tung University, Hsinchu 30050, Taiwan, Republic of China
(Received 7 October 1996)

The π-electronic excitations of graphite layers are studied within the random-phase approximation. They principally reflect the π-band characteristics, the strong wave-vector dependence, the anisotropic behavior, and the special symmetry. The π plasmons in graphite have strong dispersion relations with the transferred momentum (q). They behave as an optical plasmon in a three-dimensional electron gas at small q. Moreover, the anisotropic behavior at the plane is apparent at large q. For a single graphite layer, the π plasmons would disappear at very small q, and their frequencies are obviously reduced. The absence of interlayer Coulomb interactions is the main reason for this. The stage-1 graphite intercalation compounds (GIC's), as compared with graphite, exhibit the richer excitation spectra and the lower π-plasmon frequencies. They have the intraband plasmon as well as the interband π plasmon. These two kinds of plasmons are quite different from each other in certain respects, e.g., the cause of the plasmon. The enhanced interlayer distances could effectively reduce the π-plasmon frequency, but not the transferred charges. The calculated plasmon frequencies are consistent with the experimental measurements on graphite and stage-1 GIC's. [S0163-1829(97)05820-7]

I. INTRODUCTION

Graphite is one of the most extensively studied materials both experimentally and theoretically. Such a layered system is very suitable for the study of two-dimensional (2D) phenomena. It could be further intercalated by various atoms or molecules, which, thus, form many interesting graphite intercalation compounds (GIC's).[1] Moreover, graphite is closely related to the recently found carbon nanotubes,[2] C_{60},[3] and encapsulated C_{60}.[4] Many studies show that these systems may exhibit similar physical properties. For example, the π plasmon, the π-electronic collective excitations, is found to exist in graphite,[5–7] GIC's,[8,9] carbon nanotubes,[10] C_{60}-related materials,[11] and encapsulated C_{60}.[12] In this work, we mainly study the π plasmon in graphite and stage-1 GIC's. The dependence of the π-plasmon frequency (w_p) on magnitude (q) and direction (ϕ) of the transferred momentum, interlayer Coulomb interactions, and transferred charges is included in the study. Comparison with experimental measurements[6,8,9] is discussed.

The π and σ bands in graphite are formed, respectively, by $2p_z$ and $(2s,2p_x,2p_y)$ orbitals. The excitation properties could be measured by the electron-energy-loss spectrum[6,7] (EELS) and optical spectrum.[5] Zeppenfeld[6] and Buchner[7] measured the q-dependent transmission EELS, in which the transferred momentum is along the graphite layer. These measurements[6,7] show that the π-plasmon frequency is $\sim 7-12$ eV and the $\pi+\sigma$-plasmon frequency $\sim 27-32$ eV. For the interaction between two carbon atoms, the intralayer interaction is much larger than the interlayer interaction, owing to the large interlayer distance. Hence the model, in which graphite is regarded as a 2D supperlattice, is a reasonable first approximation. It is convenient for theoretical studies, e.g., the q-dependent π plasmon studied here. There are many 2D band-structure calculations.[13–20] They[15–18] could explain the optical properties[5] at high frequencies. In addition, the above model is successful in understanding physical properties of GIC's.[1,20,21] A single graphite layer is a zero-gap semiconductor, while graphite is a semimetal[1,14,21–23] in the inclusion of the weak interlayer interaction. Graphite has a small concentration of holes and electrons near the Fermi level. The physical properties associated with the Fermi surface are not adequately studied by the 2D supperlattice model, e.g., the intraband plasmon with a very low frequency $(\sim 0.1$ eV),[24] but not the π plasmon.

The tight-binding model[13] is used to calculate the π band, and the random-phase approximation (RPA) to study the π-electronic excitations below 15 eV. The supperlattice of infinite graphite layers is coupled by the Coulomb interactions among electrons. The interlayer Coulomb coupling is expected to play an important role in the π plasmon, since it is strong at small qI_c (I_c the periodical distance between two neighboring graphite layers). The band-structure effects are appreciable, and markedly affect the characteristics of the dielectric function $[\epsilon(q,\phi,w)]$, which is very different from that of an electron gas (EGS).[25] The calculated EELS shows that the π plasmon is characterized by the most prominent peak. The π plasmon is derived from the interband excitations from the valence to the conduction bands, and its cause will be investigated. The π-band characteristics, the strong wave-vector dependence, and the anisotropy at the plane will be reflected in the π plasmon. We study the q-dependent behavior, and under which conditions the anisotropic behavior is apparent. The calculated π-plasmon frequencies are compared with the experimental measurements.[6]

GIC's have long been extensively studied.[1,21] They are characterized by a stage index n denoting the number of the graphite layers between two intercalant layers. We focus our attention on the stage-1 GIC's $(n=1)$. When atoms or molecules are intercalated into graphite, charges would be transferred from the graphite layers into the intercalant layers. GIC's, respectively, belong to acceptor type (AGIC's) and donor type (DGIC's), if the transferred charges are electrons and holes. The intercalation is assumed to merely alter the Fermi energy E_F in the rigid band described by Eq. 2(a). AGIC's and DGIC's have similar excitation properties as a

result of the symetric π band [Fig. 1(c)]. GIC's have the high-density free carriers, which could induce the intraband excitations. Their excitation spectra are thus richer than those of graphite. In addition to the interband π plasmon, GIC's could exhibit the intraband plasmon[8,9] with frequency ~ 1 eV. Ritsko and Rice[8] measured in detail the q-dependent EELS of the stage-1 graphite $FeCl_3$ (AGIC's), and verified these two kinds of plasmons. The characteristics of the intraband plasmon have been studied theoretically.[26,27] However, the intraband excitations and the π plasmons in GIC's are not fully understood. The details concerning the intraband excitations need to be further clarified, e.g., the ϕ-dependent excitation properties and the cause of the intraband plasmon. The stage-1 GIC's, as compared with graphite,[6] exhibit the lower π-plasmon frequency.[8] The effects due to the transferred charges and the enhanced interlayer distances will be investigated. There are certain EELS measurements[9] on the stage-1 C_8M (M stands for K, Rb, and Cs; DGIC's), but at $q=0.1$ Å^{-1}. The π plasmons in these stage-1 DGIC's are also studied.

This paper is organized as follows. In Sec. II, the dielectric functions of graphite and stage-1 GIC's are calculated within the RPA. The excitation properties of the π electrons are studied in Sec. III. The calculated π-plasmon frequencies are compared with the experimental measurements.[6,8,9] Concluding remarks are given in Sec. V.

II. THE DIELECTRIC FUNCTION

The π band of a graphite layer is simply reviewed. It is obtained from the tight-binding model established by Wallace.[13] Both energy dispersions and Bloch functions are analytic; therefore, they are convenient in calculating the dielectric function. The positions of carbon atoms are characterized by the two primitive lattice vectors, $\mathbf{a}_1$ and $\mathbf{a}_2$ [Fig. 1(a)]. The $2p_z$ orbitals belong to two sublattices, so the Bloch states could be described by the combination of the two tight-binding functions $U_1(k_x,k_y)$ and $U_2(k_x,k_y)$. The Hamiltonian with only the nearest-neighbor interactions is further given by

$$H=\begin{pmatrix} 0 & H_{12}(k_x,k_y) \\ H_{12}^*(k_x,k_y) & 0 \end{pmatrix}, \tag{1a}$$

where

$$H_{12}(k_x,k_y)=-\gamma_0\left\{e^{-ik_yb}+2e^{ibk_y/2}\cos\left(\frac{\sqrt{3}bk_x}{2}\right)\right\}. \tag{1b}$$

$b=1.42$ Å is the C-C bond length. The resonance integral $\gamma_0=2.5$ eV is taken from the comparison between the tight-binding model and the local-density approximation.[19] Other calculations could also obtain similar values ($\gamma_0 \sim 2.3$–2.7 eV).[14,18,20,23,28] Diagonalizing the Hamiltonian, the energy dispersions are

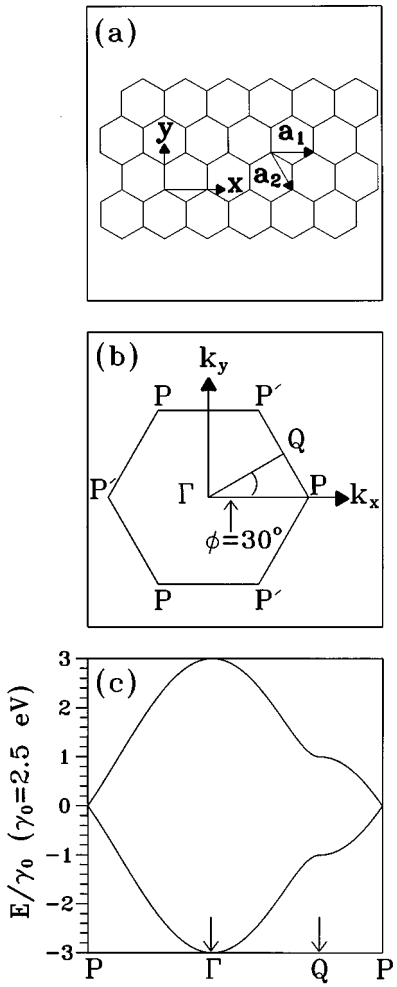

FIG. 1. (a) A single graphite layer. (b) The first Brillouin zone. The Γ point is the origin. The P and P' points are the corners, and the Q point is the middle point between them. (c) The 2D π band.

$$E^{c,v}(k_x,k_y)=\pm\gamma_0\left\{1+4\cos\left(\frac{3bk_y}{2}\right)\cos\left(\frac{\sqrt{3}bk_x}{2}\right)+4\cos^2\left(\frac{\sqrt{3}bk_x}{2}\right)\right\}^{1/2}, \tag{2a}$$

and the Bloch functions are

$$\Psi^{c,v}(k_x,k_y)=\frac{1}{\sqrt{2}}\left\{U_1(k_x,k_y)\pm\frac{H_{12}^*(k_x,k_y)}{|H_{12}(k_x,k_y)|}\,U_2(k_x,k_y)\right\}. \tag{2b}$$

The superscript c (v) represents the conduction (valence) band. The wave vectors k_x and k_y are confined within the first Brillouin zone [BZ; Fig. 1(b)]. A single graphite layer is a zero-gap semiconductor, as shown in Fig. 1(c). The corners (P or P' points) and the middle points (Q points) between them are critical points in the energy-wave-vector space. It is noticed that critical points include minima, maxima, and saddle points. The excitations from the critical points could induce the singular structures in the dielectric functions (Sec. III). The π band is anisotropic at the plane, and so are the π-electronic excitations. The Fermi level of the stage-1 AGIC's (DGIC's) is inside the valence (conduction) band within

the 2D rigid-band model. AGIC's and DGIC's would exhibit similar excitation spectra owing to the symmetric π band. The energy dispersion relations are linear and isotropic in the neighborhood of the P and P' points. Blinowski *et al.*[20] further proposed a linear energy band by using these two characteristics. Such a simple band is successful in understanding optical and electronic properties of GIC's.[1,21] For example, it is utilized[27] to explain the intraband plasmon in the stage-1 graphite $FeCl_3$.[8] Here the rigid band in Eq. (2) is used to study the π plasmons in the stage-1 AGIC's and DGIC's. In short, the π band exhibits the following characteristics: strong wave-vector dependence, anisotropy, and special symmetry. They will be directly reflected in the excitation spectra.

The π-electronic excitations are described by magnitude (q) and direction (ϕ) of the transferred momentum and excitation energy (w). $0° \leqslant \phi \leqslant 30°$ is sufficient to characterize the various direction-dependent excitations because of the hexagonal symmetry. The response function (χ) is calculated from the self-consistent-field method (RPA).[29] For a single graphite layer, the dielectric function is given by

$$\epsilon^{2D}(q,\phi,w) = \epsilon_0 - V_q \chi(q,\phi,w), \tag{3a}$$

$$\chi(q,\phi,w) = 2 \sum_{h,h'=c,v} \int_{1\text{st BZ}} \frac{dk_x dk_y}{(2\pi)^2} |\langle k_x+q_x, k_y+q_y; h'|e^{iq_x x} e^{iq_y y}|k_x, k_y; h\rangle|^2 \times \frac{f(E^{h'}(k_x+q_x, k_y+q_y)) - f(E^h(k_x,k_y))}{E^{h'}(k_x+q_x,k_y+q_y) - E^h(k_x,k_y) - (w+i\Gamma)}, \tag{3b}$$

where[27]

$$|\langle k_x+q_x, k_y+q_y; h'|e^{iq_x x} e^{iq_y y}|k_x, k_y; h\rangle|^2 = \tfrac{1}{4}\{1+q^2/36\}^{-6} \left| 1 \pm \frac{H_{12}(k_x+q_x,k_y+q_y) H_{12}^*(k_x,k_y)}{|H_{12}(k_x+q_x,k_y+q_y) H_{12}^*(k_x,k_y)|} \right|^2. \tag{3c}$$

$q_x = q\cos\phi$ and $q_y = q \sin\phi$. $\epsilon_0 = 2.4$ is the background dielectric constant.[5] $V_q = 2\pi e^2/q$ is the Coulomb interaction of a 2D EGS. f is the Fermi distribution function. It is sufficient to consider the $T=0$ case, because the plasmon frequency (>1 eV) is much larger than the thermal energy. $+$ and $-$ in Eq. (3c), respectively, correspond to the intraband ($v \to v$ and $c \to c$) and the interband ($v \to c$ and $c \to v$) excitations. The response function in Eq. (3b) has included the band-structure effect on the Coulomb interaction [Eq. (3c)]. There exist electron-hole (e-h) excitations when $\mathrm{Im}\chi \neq 0$. The intraband excitations are clearly absent in a graphite layer with $E_F = 0$; i.e., they are absent in graphite, but present in GIC's. Graphite and GIC's thus have different excitation spectra, as shown in Figs. 2(a) and 2(b). The details concerning the π-electronic excitations will be discussed in Sec. III. Γ is the energy width due to various deexcitation mechanisms. It could cause the broadening effect of the excitation spectrum. The excited electrons could further decay by means of the electron-electron interaction,[27] the electron-phonon interaction, the electron-impurity scattering, and the electron-intercalant scattering. The energy width generally depends on the wave vector, and it is predicted to ~ 0.1 eV for the inelastic Coulomb scattering.[27] Γ here is treated as a free parameter, and $\Gamma = 0.1$ eV is mainly taken in the calculations. $\Gamma = 2$ meV used in the inset of Fig. 7 is only for clarifying the special structures of ϵ before broadening. When Γ is finite, χ needs to be replaced by[30]

$$\chi(q,\phi,w) = \frac{(1+i\Gamma/w)\chi(q,\phi,w+i\Gamma)}{1+(i\Gamma/w)[\chi(q,\phi,w+i\Gamma)/\chi(q,\phi,w=0)]}. \tag{4}$$

The above correction does not lead to significant changes in the excitation properties, e.g., the π-plasmon frequencies.

Both graphite and stage-1 GIC's are regarded as 2D supperlattices, which are composed of the infinite periodical graphite layers. Each layer has the π band described by Eq. (2a) and the response function by Eq. (3b). Excitations on a certain layer are screened by electrons on all layers via the Coulomb interactions. The interlayer coupling is very important in supporting the π plasmon at $q \to 0$ and enhancing the plasmon frequency. This supperlattice model is similar to that of the layered EGS.[31] The difference in the electronic structure is what distinguishes these two systems.

The dielectric function [Eq. (3a)] of a single graphite layer would be modified in the presence of the interlayer Coulomb interactions. Graphite and stage-1 GIC's are assumed to be perturbed by a probing electron with the time-dependent potential $V^{ex}(q,\phi,w)$. Electrons on all layers will screen this external field, which thus causes the induced charges. The effective potential (V^{eff}) is the sum of the external potential and the induced potential from all induced charges. V_l^{eff} on the lth layer is given by[31]

$$\begin{aligned} \epsilon_0 V_l^{eff}(q,\phi,w) &= V_l^{ex}(q,\phi,w) + V_l^{in}(q,\phi,w) \\ &= V_l^{ex}(q,\phi,w) \\ &\quad + \sum_{l'} V_{l,l'}(q) V_{l'}^{eff}(q,\phi,w) \chi(q,\phi,w), \end{aligned} \tag{5}$$

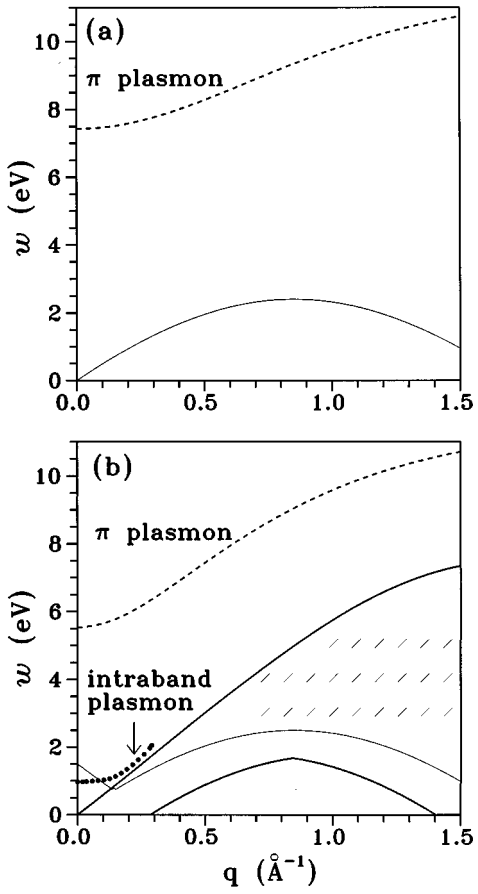

FIG. 2. (a) The excitation spectrum of graphite is shown at $\phi=0°$. The heavy dashed curve corresponds to the π plasmon of the $q_z=0$ mode. The region above the light solid curve is the interband e-h excitations. (b) Same plot as (a), but for the stage-1 GIC's, with $E_F=0.75$ eV and $I_c=9.42$ Å. The dotted curve is the intraband plasmon. The region bound by the two heavy solid curves is the intraband e-h excitations. The shaded region is the coexistent region including the interband and intraband e-h excitations.

where $V_{l,l'}(q)=V_q\exp(-q|l-l'|I_c)$ is the interlayer Coulomb interaction. $V_{l'}^{\rm eff}\chi$ is recognized to be the induced charge density on the l'th layer. Equation (5) could be solved by performing the following Fourier transform:

$$\sum_l V_l^{\rm ex}(q,\phi,w)e^{iq_z lI_c}=V^{\rm ex}(q,\phi,w;q_z), \tag{6}$$

where $|q_zI_c|\leq\pi$, and similarly for $V_l^{\rm eff}$. The effective potential is further given by

$$V_l^{\rm eff}(q,\phi,w)=\frac{I_c}{2\pi}\int_{-\pi/I_c}^{\pi/I_c}dq_z\,\frac{V^{\rm ex}(q,\phi,w;q_z)}{\epsilon_0-V_qS(q;q_z)\chi(q,\phi,w)}, \tag{7a}$$

where

$$S(q;q_z)=\sinh(qI_c)/[\cosh(qI_c)-\cos(q_zI_c)]. \tag{7b}$$

$S(q;q_z)\approx1$ at large qI_c, which means that the interlayer Coulomb coupling and the differences among various q_z's modes are negligible.

The effective potential in Eq. (7a) depends on the external potential, namely, the density distribution of the probing electron. There are two kinds of special cases. First, the density distribution inside the system is uniform if the probing electron has the well-defined momentum state. $V_l^{\rm ex}$ is independent of l so that the $q_z=0$ mode is the only effective excitation mode. The effective dielectric function is then expressed by

$$\epsilon(q,\phi,w)=\frac{V_l^{\rm ex}(q,\phi,w)}{V_l^{\rm eff}(q,\phi,w)}=\epsilon_0-V_qS(q;q_z=0)\chi(q,\phi,w). \tag{8}$$

Second, the probing electron is localized on the $l=0$ layer, i.e., $V_{l=0}^{\rm ex}=V_q$. All the q_z modes would contribute to the excitation spectra, but have different weight. The effective dielectric function is expressed by

$$\epsilon(q,\phi,w)=\frac{V_{l=0}^{\rm ex}(q,\phi,w)}{V_{l=0}^{\rm eff}(q,\phi,w)}=\sqrt{B^2-1}\,\mathrm{sgn}[\mathrm{Re}B]/\sinh(qI_c), \tag{9a}$$

where

$$B=\cosh(qI_c)-\sinh(qI_c)V_q\chi(q,\phi,w)/\epsilon_0. \tag{9b}$$

The momentum resolution (Δk) is, respectively, 0.033 and 0.055 Å^{-1} in the measurements of graphite ($I_c=3.35$ Å) (Refs. 6 and 7) and stage-1 graphite $FeCl_3$ ($I_c=9.42$ Å).[8] The wave-packet width ($>1/\Delta k$) of the probing electron is roughly estimated to be larger than the periodical distance I_c. The dielectric function only with the $q_z=0$ mode [Eq. (8)] is relatively appropriate in describing excitation properties, and is primarily used in the calculations. But, basically, excitation spectra are similar for the above two kinds of dielectric functions.

III. THE π PLASMONS

The dielectric function in Eq. (8) is mainly used to study excitation properties of the graphite layers, e.g., the effect of band structure on ϵ and the q- and ϕ-dependent π plasmons. The π-plasmon frequencies are evaluated for graphite and stage-1 GIC's, and the calculated results are compared with the experimental measurements.[6,8,9]

A. Graphite

For a single graphite layer, the interband excitations from the valence to the conduction bands are the only effective excitation channel. Graphite has only interband excitations, if the weak overlap[1,21] between the valence and the conduction bands is neglected. The excitation spectrum of graphite along the x axis ($\phi=0°$) is shown in Fig. 2(a). The excitations from the P points [Fig. 1(b)] require the minimum energy, the threshold energy $E_{\rm th}$ (the light solid curve). It must have the interband e-h excitations, when excitation energies are higher than $E_{\rm th}$. Moreover, the π plasmon (the heavy dashed curve) survives in the interband e-h excitations, which is damped even at very small q. These excitation properties are in great contrast to those of an EGS.[25] For example, the e-h excitations of an EGS are seriously limited by the Fermi surface, and the plasmon is undamped at small

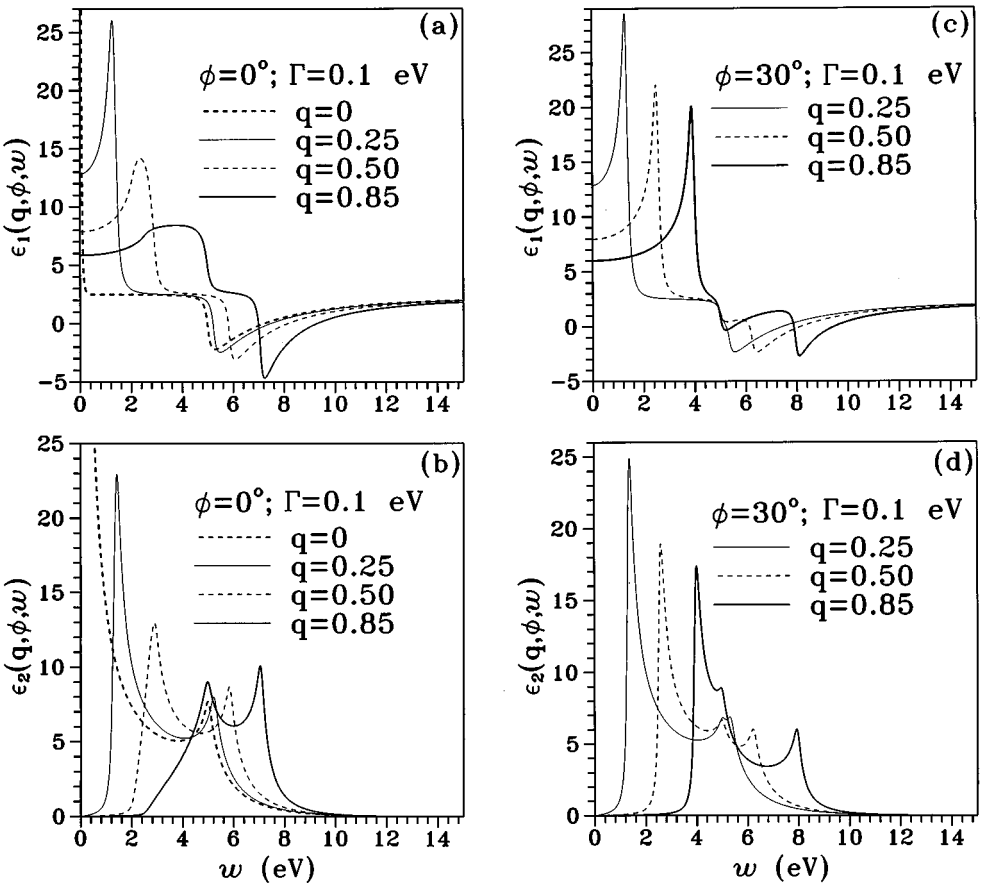

FIG. 3. The dielectric function ϵ of the $q_z=0$ mode. (a) The real part ϵ_1 for various q at $\phi=0°$ and $\Gamma=0.1$ eV. (b) Same plot as (a), but for the imaginary part ϵ_2. (c) Same plot as (a), but calculated at $\phi=30°$. (d) Same plot as (a), but for ϵ_2 at $\phi=30°$. The units of q is Å^{-1} here and henceforth.

q. The boundary of the interband e-h excitations is elevated with increasing ϕ (not shown), and so is the π plasmon frequency [Fig. 5(a)]. The excitation spectra are basically similar for various azimuthal angles.

The dielectric function [Eq. (8)] for various q at $\phi=0°$ and $\Gamma=0.1$ eV is shown in Figs. 3(a) and 3(b). We first see the $q\rightarrow 0$ case. The imaginary part of the dielectric function [ϵ_2; the heavy dashed curve in Fig. 3(b)] exhibits a divergent peak at $w\rightarrow 0$. ϵ_2 is proportional to Imχ [Eq. (3b)], so the singular structure is derived from the characteristics of the interband excitation energy $[w_{vc}=E^c(k_x+q_x,k_y+q_y)-E^v(k_x,k_y)]$ in the energy-wave-vector space. w_{vc} near the P or P' points is isotropic and linear at very small q. The π-band model[20] of Blinowski *et al.* is used to study the singular structure in ϵ. ϵ_2 obtained from this model diverges in the form $1/\sqrt{w-w_0}$,[27] where $w_0=3\gamma_0 bq/2$ is very close to E_{th}. By using the Kramers-Kronig relations, the real part of the dielectric function [ϵ_1; the heavy dashed curve in Fig. 3(a)] further diverges in the form $1/\sqrt{w_0-w}$. At $w=2\gamma_0$, ϵ_2 exhibits another singular structure, a logarithmic divergency. It results from the excitations of the middle points (the Q points) between P and P' points, since these critical points are saddle points in the energy-wave-vector space.[32] Concomitant with the logarithmic divergency in ϵ_2 is a discontinuity (a diplike structure after broadening) in ϵ_1. ϵ_1 is negative near this structure, and then it would become vanishing. The zero of ϵ_1, if at where ϵ_2 is small, is associated with the π plasmon of graphite. The plasmon could induce a prominent peak in EELS (Fig. 4).

When q increases from zero, P and P' points have different characteristics. The P point remains at a minimum. The excitation matrix element in Eq. (3c) vanishes; therefore, there is no singular structure at the threshold energy. However, the P' point gradually changes from a minimum into a saddle point with increasing q. The singular structure in ϵ_2 (ϵ_1) would alter from the square-root divergency into the logarithmic divergency (the barrierlike structure). On the other hand, the singular structures at high frequencies keep their forms as q increases. That is to say, ϵ_2 always exhibits the logarithmic divergency and ϵ_1 the diplike structure at $w\geqslant 2\gamma_0$. They are due to the saddle points, which satisfy the condition $\partial w_{vc}/\partial k_x=0$ and $\partial w_{vc}/\partial k_y=0$. These saddle points would vary with q, which contrast strongly with the fixed saddle point P'. They are just the Q points at $q=0$, but the former are gradually away from the latter when q grows. The excitations from such saddle points could lead to diplike structures and zeroes in ϵ_1, so that they are recognized to be the cause of the π plasmon. It is interesting to note that similar inter-π-band excitations have been suggested to explain the $\sim$6-eV π plasmon in C_{60}-related materials[11] and carbon nanotubes.[33] The frequencies corresponding to the vanishing ϵ_1 are enhanced with increasing q. The π plasmon frequencies are thus expected to increase with q.

The excitation properties also depend on the direction of the transferred momentum. ϕ would affect the number and

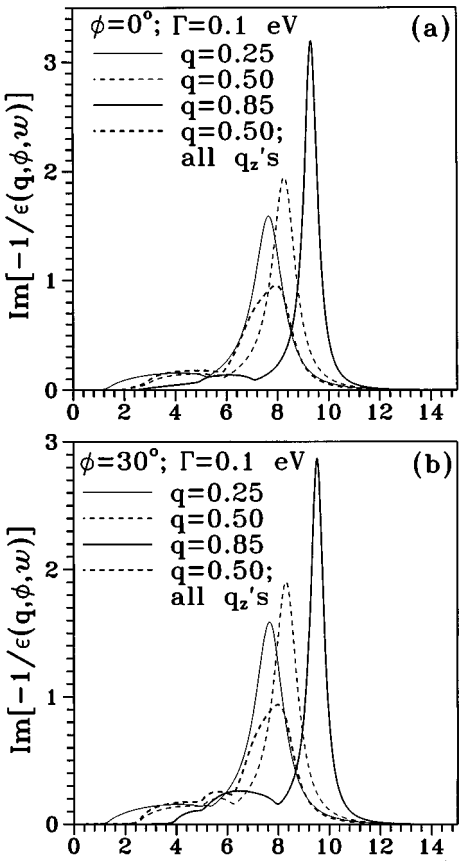

FIG. 4. The EELS are calculated from ϵ shown in Figs. 3(a)–3(d). That (the heavy dashed curve) including all q_z modes at $q=0.5$ Å^{-1} is also shown for comparison. (a) $\phi=0°$ and (b) $\phi=30°$.

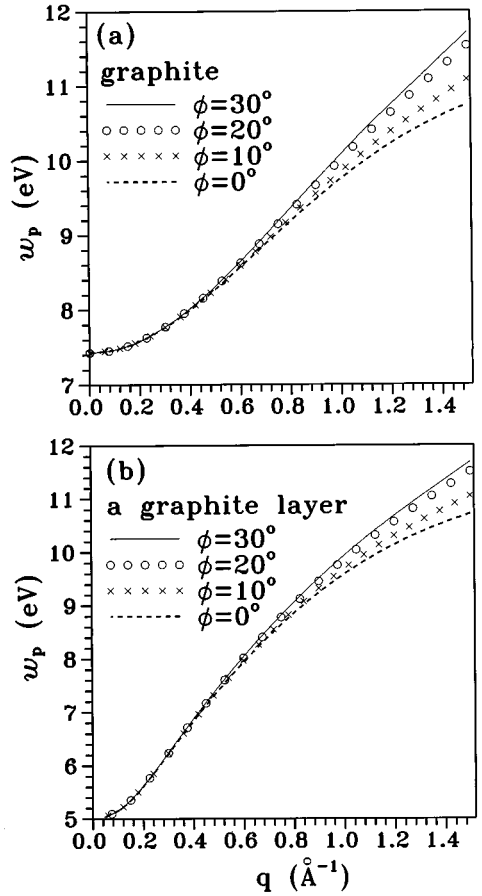

FIG. 5. (a) The π-plasmon frequencies of the $q_z=0$ mode are calculated at various ϕ for graphite. Same plot as (b), but for a single graphite layer.

the positions of the critical points. ϵ at $\phi=30°$ [Figs. 3(c) and 3(d)] is taken as an example. When ϕ increases from zero to 30°, the characteristics of the P and P' points become the same. Both of them are minima at $\phi=30°$. The excitations from the P and P' points could cause the sharp excitation edge in ϵ_2 at any q. Moreover, ϵ_2 and ϵ_1 exhibit the square-root divergencies at the threshold energy.[27] There are two more singular structures at $w \geq 2\gamma_0$, which are caused by two different saddle points. These saddle points are close to the Q points at small q, as stated above. The number of saddle points is determined by the topological considerations, and here it depends on ϕ and q. The diplike structures or the zeros of ϵ_1 [Fig. 3(c)] occur at higher frequencies as compared with those of ϵ_1 in Fig. 3(a). The π plasmons, as indicated from this result, have higher frequencies at larger ϕ (Fig. 5). In brief, the singular structures in the dielectric function directly respond to the special symmetry of the π band, and are appreciably affected by q and ϕ.

Zeppenfeld[6] first measured the q-dependent transmission EELS at $\phi=0°$ and 30°, and obtained ϵ_1 and ϵ_2 from the Kramers-Kronig relations. Buchner[7] later made similar measurements, and obtained similar ϵ_2. Zeppenfeld's result is complete, and is used as a model for discussion. The experimental (Figs. 10 and 11 in Ref. 5) and the theoretical [Figs. 3(a)–3(d)] results are consistent with each other in the forms and the number of the singular structures. The magnitude of ϵ is similar; moreover, the differences between the positions of the singular structures are within the experimental energy resolution (>0.5 eV).

The EELS, defined as $\mathrm{Im}[-1/\epsilon(q,\phi,w)]$, is calculated for a closer study of the π plasmon. The results for various q at $\phi=0°$ are shown in Fig. 4(a). Each spectrum exhibits a weak and a broad peak at low w, and a very pronounced peak at $w>7$ eV. The former is due to the e-h excitations. The latter is identified as the π plasmon, since it results from the vanishing ϵ_1 and the small ϵ_2 [Figs. 3(a) and 3(b)]. The plasmon peak remains strong even at large energy width, e.g., $\Gamma=0.5$ eV. This band-induced plasmon mode is the most important excitation in the loss spectrum. The π plasmon frequency clearly increases as q grows [Fig. 5(a)]. EELS will remain similar during the variation of ϕ. The increasing ϕ only changes the detailed EELS. It could enhance the number and the intensity of the weak peaks, and the π plasmon frequency, but reduce the intensity of the π plasmon peak, e.g., EELS at $\phi=30°$ [Fig. 4(b)].

The measured EELS depends on the probing electron (or the external potential) in addition to the intrinsic response function, as discussed in Sec. II. The above-mentioned EELS are the excitation spectra of the $q_z=0$ mode. They correspond to the uniformly probing electron density. But when the probing electron is localized on a certain layer, all q_z modes are effective excitation channels. The plasmon is a

quantum of the electronic collective oscillation. The plasma oscillations on all layers are in phase for the $q_z=0$ mode, which would exhibit the strongest plasmon peak and the highest plasmon frequency. In general, for small $|q_z|$ modes, the plasmon peaks are stronger, and the plasmon frequencies are higher.[31] The differences among various q_z modes are primarily decided by the factor $S(q;q_z)$ in Eq. (7b). They are obvious at small q, but negligible at large $q(\geq 1\ \text{Å}^{-1})$. The EELS including all q_z modes [the heavy dashed curves in Figs. 4(a) and 4(b)], as compared with those of the $q_z=0$ mode, would exhibit weaker plasmon peaks at lower frequencies. The measured EELS are expected to be between the above two kinds of EELS.

We further see the dispersion relation of plasmon frequency with q. $w_p(q)$ of the $q_z=0$ plasmon mode at various ϕ is shown in Fig. 5(a). The strong q dependence directly reflects the π-band characteristic, the strong wave-vector dependence. It approaches a finite value at $q\rightarrow 0$; therefore, the π plasmon in graphite belongs to an optical plasmon. Furthermore, w_p at small q is examined to be well fitted by $C_0+C_2q^2$. The π plasmon indicated from such behavior is like an optical plasmon in a 3D EGS,[25] even if they respectively correspond to the interband and the intraband excitations. The q-dependent plasmons also rely on ϕ. The dielectric function, as seen in Figs. 3(a)–3(d), at any q is obviously influenced by ϕ. However, the dependence of w_p on ϕ is strong only at large q; i.e., the π plasmon would clearly exhibit the anisotropic behavior under such a condition.

The π plasmon in a single graphite layer [Fig. 5(b)] is also studied to understand the effects of the interlayer Coulomb interactions. There are two principal differences between a 2D graphite layer and graphite. One is that the π plasmons at very small q $(q<0.05\ \text{Å}^{-1})$ would disappear in the former, while they could exist in the latter. Such π plasmons in a single graphite layer are completely suppressed by the interband e-h excitations. It means that at the long-wavelength limit, the interlayer Coulomb interactions are very important in supporting the π plasmon of graphite. Additionally, these interactions play a similar role in the intraband plasmons of the stage-1 GIC's (see below).[26,27] Also the plasmon frequencies of the former are much lower than those of the latter at small q $(q<0.5\ \text{Å}^{-1})$; that is, w_p's are considerably enhanced by the interlayer Coulomb interactions. The main reason for this is that the interlayer Coulomb coupling is very strong at small qI_c.

The calculated plasmon frequencies could provide a reasonable explanation for the experimental measurements. Zeppenfeld[6] measured the q-dependent π-plasmon frequencies for various q's at $\phi=0°$ (squares in Fig. 6) and $\phi=30°$ (circles). The experimental energy resolution is ~ 0.5 eV at small q and even lower at large q.[7] The plasmon frequencies are dependent on the external potential, since the wave packet of the probing electron has a finite width. The uniform and the localized probing electrons, respectively, result in the excitations of the $q_z=0$ mode and all q_z modes. $w_p(q)$ of the former is higher than that of the latter, as stated earlier. Their frequency difference is mainly at small q, and it is ~ 0.35 eV at $q\rightarrow 0$. The calculated results are approximately estimated to be the plasmon frequencies between those of the $q_z=0$ mode and all q_z modes. They are consistent with the experimental results. This is a good indication

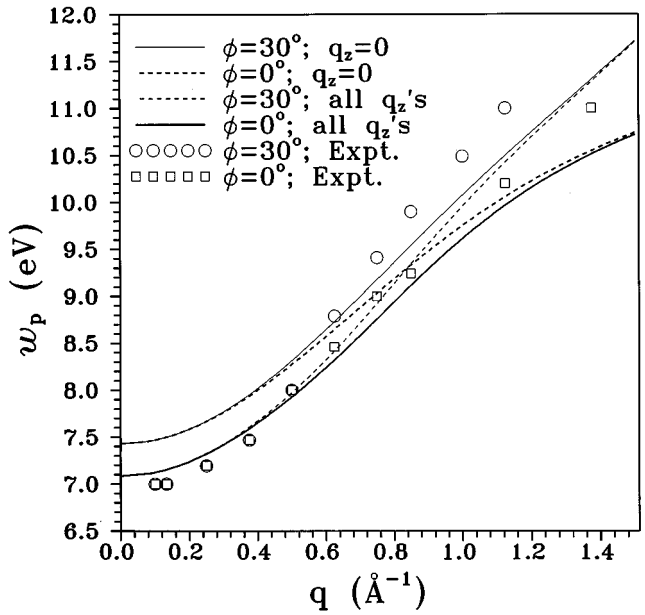

FIG. 6. The π-plasmon frequencies of $q_z=0$ mode and all q_z modes are calculated at $\phi=30°$ and $\phi=0°$. The calculated results are compared with the experimental measurements (Ref. 6).

of the suitability of the 2D supperlattice model for graphite. In addition, the π-plasmon frequencies of the semi-infinite graphite were measured by the reflection EELS.[34] The q dependence of w_p is almost absent, which is in great contrast to the measured results of the transmission EELS.[6,7] Whether the surface markedly affects the π-plasmon frequencies needs further experimental and theoretical studies.

B. Stage-1 GIC's

GIC's could exhibit the intraband and the interband excitations, which differ greatly from graphite. The intercalation would change the Fermi energy and the interlayer distances. Its effects on the excitation properties are investigated. Ritsko and Rice[8] measured the EELS of the stage-1 graphite $FeCl_3$ (AGIC's), and obtained the q-dependent π plasmon frequencies. The 2D supperlattice model is used to explain the measured results. In general, the 2D rigid-band model is relatively suitable for the AGIC's.[1,20,21] We also study the π plasmon in the stage-1 C_8M (DGIC's). Comparison with experimental measurements[9] is useful in understanding whether such a model is suitable for these compounds.

The stage-1 graphite $FeCl_3$, with $E_F=0.75$ eV and $I_c=9.42$ Å,[27] is taken as an example. The excitation spectrum at $\phi=0°$ is shown in Fig. 2(b). GIC's, as compared with graphite [Fig. 2(a)], exhibit the richer spectrum. In addition to the interband e-h excitations and the π plasmon, GIC's could exhibit intraband e-h excitations and the plasmon. The intercalation has certain important effects on the excitation spectra. First, the intraband excitations are present in GIC's, while they are absent in graphite. They are apparently due to free holes in AGIC's. The boundaries (the heavy solid curves) of the intraband e-h excitations are determined by the Fermi surface. Moreover, the intraband plasmon in GIC's is undamped at sufficiently small q $(<0.1\ \text{Å}^{-1})$, and vice versa. Second, the interband threshold energies (the light

solid curves) at small q are comparatively high for GIC's. The interband excitations in GIC's are limited by the Fermi surface states; hence, they need higher excitation energies. The threshold excitations result from the Fermi surface states for GIC's, but the P point for graphite. Also notice that the interband threshold energies at large q are the same for GIC's and graphite, i.e., they correspond to the P point. Finally, the π-plasmon frequencies in GIC's are obviously reduced. The main reason is shown to be the enhanced interlayer distances (see below).

The excitation spectrum would alter with ϕ. Its main change is the coexistent region including the intraband and the interband e-h excitations [the shaded region in Fig. 2(b)]. The coexistent feature principally reflects the fact that the P and P' points have different excitation properties at $\phi \neq 30°$ (see below). When ϕ increases from zero, such a region would gradually diminish and finally disappear at $\phi = 30°$ (not shown). Mele and Ritsko[26] used the 2D π-band structure to study the low-frequency excitation spectrum. They obtained the coexistent region similar to Fig. 2(b) at $\phi = 0°$. On the other hand, Shung[27] used the linear and isotropic π-band structure,[20] so the coexistent region did not exist. The boundary of the interband e-h excitations just touches the upper boundary of the intraband excitations, which is similar to the $\phi = 30°$ case.

The dielectric function at $q = 0.21$ Å^{-1} and $\phi = 0°$ is shown in Figs. 7(a) and 7(b). The contribution from the intraband excitations is confined to the low-frequency range (the solid curves in insets), since the momentum and the energy are conserved in the electron-electron interaction. At $\phi = 0°$, the Fermi surface states near the P point are quite different from those near the P' point. A certain Fermi surface state near the P point is a saddle point, and that near the P' point is a maximum. For $\epsilon_2(\epsilon_1)$, they respectively cause the logarithmic divergency[32] (the discontinuity or the diplike structure after broadening) and the positive square-root divergency[27] (the negative square-root divergency or the diplike structure). The intraband excitation from the maximum could result in a zero of the total ϵ_1 [the heavy dashed curve in the inset of Fig. 7(a)] at small ϵ_2 and thus are related to the intraband plasmon. Additionally, this plasmon may be damped by the interband e-h excitations because of $\epsilon_2 \neq 0$ [the light dashed curve in the inset of Fig. 7(b)].

Concerning the interband excitations, the roles of the P and P' points may be similar to those in graphite. The former is a minimum, and the latter is a saddle point. There is another saddle point, which originates from a certain Fermi surface state close to the P point. Its excitation energy is between those of P and P' points. The above two saddle points[32] induce the logarithmic divergences in ϵ_2 and the barrierlike structures in ϵ_1. Here, the minimum interband excitation energy of the P point is relatively small, as compared with the maximum intraband excitation energy of the Fermi surface states near the P' point. Hence the interband excitations could coexist with the intraband excitations at a certain region [inset in Fig. 7(b)]. The coexistent feature is subject to the following conditions: the excitation properties near the P point differ from those near the P' point, and the P point is the minimum of the interband excitations. On the other hand, when q is sufficiently small ($q < 0.15$ Å^{-1}), a certain Fermi surface state close to the P point would become a minimum. This implies that the interband e-h excitations are located above the intraband e-h excitations [Fig. 2(b)], or the coexistent region does not exist. This is also the reason the interband threshold energies of GIC's are higher than those [Fig. 2(a)] of graphite at small q. For the high-frequency excitations, the diplike structure in ϵ_1 and the logarithmic divergency in ϵ_2 stem from the saddle points near the Q points, as shown in graphite [Figs. 3(a)–3(b)].

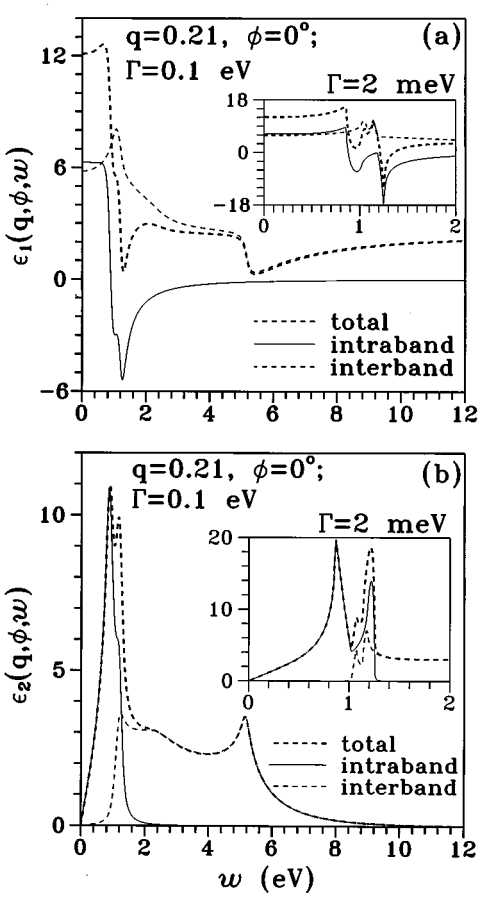

FIG. 7. The dielectric function of the stage-1 GIC's with $E_F = 0.75$ eV and $I_c = 9.42$ Å. The same GIC's are studied in Figs. 8 and 9. ϵ of the $q_z = 0$ mode is calculated at $q = 0.21$ Å^{-1}, $\phi = 0°$, and $\Gamma = 0.1$ eV. The total, intraband, and interband excitations, respectively, correspond to the heavy dashed, solid, and light dashed curves. (a) ϵ_1, and (b) ϵ_2. ϵ_1 and ϵ_2 at $\Gamma = 2$ meV are shown in the insets for clarity.

The total excitations (the heavy dashed curves) at high frequencies are hardly affected by the intraband excitations, e.g., the zero of ϵ_1. This indicates that the π-plasmon frequencies of the stage-1 GIC's are independent of the free-carrier density or the Fermi energy. The similar dielectric functions could be obtained for other q. But when q increases, the diplike structure in ϵ_1, which corresponds to the intraband plasmon, becomes shallow quickly. The intraband plasmon would disappear at the critical momentum $q_c \sim 0.3$ Å^{-1} [Fig. 2(b)]. ϵ is also affected by ϕ—mainly the number and the positions of the critical points. For example, P and P' points have similar characteristics at $\phi = 30°$, so there is no coexistent feature in the excitation spectrum.

The EELS for various q at $\phi = 0°$ is shown in Fig. 8. There are two pronounced peaks at small q, e.g., EELS at

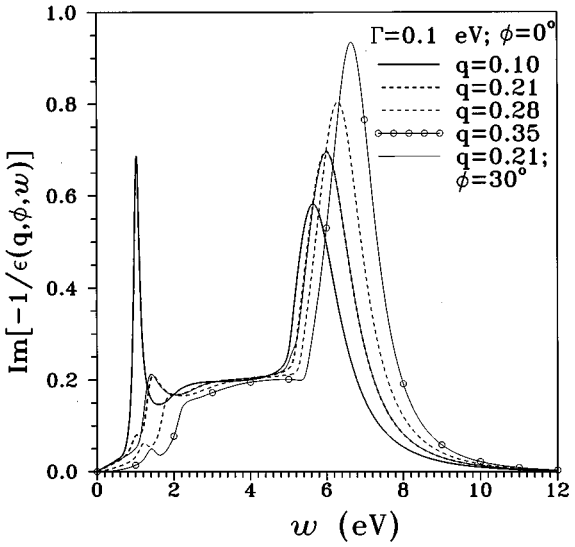

FIG. 8. The EELS of the stage-1 GIC's are calculated at various q, $\Gamma=0.1$ eV, and $\phi=0°$. That at $q=0.21$ Å^{-1} and $\phi=30°$ (the light solid curve) is also shown for comparison.

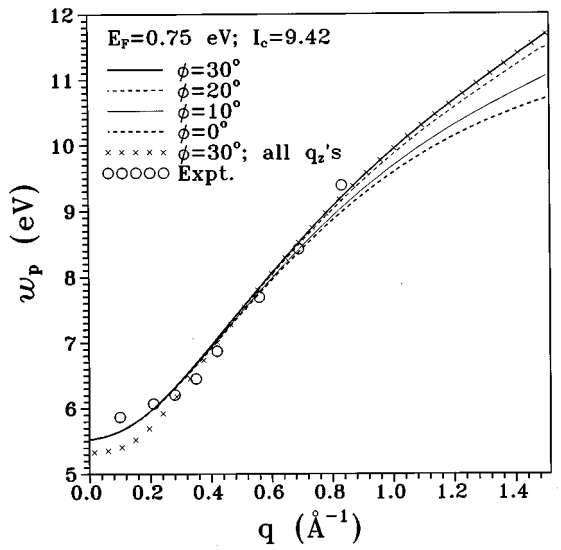

FIG. 9. The π-plasmon frequencies of the stage-1 GIC's, which correspond to the $q_z=0$ mode, are calculated at various ϕ. Those including all q_z modes are also calculated at $\phi=30°$ (the crosses) for comparison. They are compared with the experiment results (the open circles; Ref. 8). The unit of I_c is Å here and henceforth.

$q=0.1$ Å^{-1} (the heavy solid curve). The sharp peak at low frequency and the broad and strong peak at high frequency are, respectively, identified as the intraband plasmon and the π plasmon. Both of them are optical plasmons as a result of the interlayer Coulomb interactions. However, their causes and certain characteristics are very different from each other. The intraband plasmon is associated with the intraband excitations from the Fermi surface states near the P' points (also including the P points at $\phi=30°$), but the π plasmon is associated with the interband excitations from saddle points near the Q points. These two kinds of plasmons are damped by the interband e-h excitations, while the intraband plasmon is undamped at sufficiently small q [Fig. 2(b)]. Moreover, the intraband plasmon is rapidly damped down with increasing q, and its critical momentum (~ 0.3 Å^{-1}) is much smaller than that (~ 1.5 Å^{-1}) of the π plasmon. There is another weak peak at low frequency when q grows. It is the e-h excitations, and is caused by the different excitation properties around the P and P' points. This structure is absent at $\phi=30°$, e.g., EELS at $q=0.21$ Å^{-1} (the light solid curve). The measured EELS (Ref. 8) is comparatively similar to the $\phi=30°$ case. Other details concerning the intraband plasmon could be found in Refs. 26 and 27. As a general rule, the intraband plasmon behaves as an optical plasmon, with a small q_c, and its dependence on ϕ is weak.

The q-dependent π-plasmon frequencies of the stage-1 graphite $FeCl_3$ are shown in Fig. 9. The dependence of w_p on the external potential is weak, owing to the large interlayer distance $I_c=9.42$ Å. Hence $w_p(q)$ of the $q_z=0$ mode is close to that of all q_z modes except at very small q, e.g., $w_p(q)$ at $\phi=30°$. Ritsko and Rice measured w_p at various q (open circles),[8] in which the ϕ dependence was neglected. The measured and the calculated results are relatively consistent with each other at $\phi=30°$, as seen in EELS. The π plasmons in GIC's are similar to those in graphite [Fig. 5(a)] except that their frequencies are obviously reduced at small q. For example, they are like an optical plasmon in a 3D EGS at small q, and the ϕ dependence is apparent at large q.

The two factors, the interlayer distances and the transferred charges, are investigated to account for the reduced π-plasmon frequencies. They could be varied by means of intercalation.[1] The π-plasmon frequencies, as shown in Fig. 10, are strongly affected by the interlayer distances. The larger I_c is, the lower w_p is. The effect of I_c on w_p is principally decided by the interlayer Coulomb coupling [V_qS in Eq. (8)]. The interlayer interaction is reduced with increasing qI_c, so that ϵ_1 would vanish at the lower frequency. Hence, the π-plasmon frequency decreases with increasing I_c. On the other hand, the π-plasmon frequencies are insensitive to the Fermi energy. Also notice that the opposite is true for the intraband plasmon.[26,27] The screening effects due to the free carriers are confined to the low-frequency range [Fig. 7(a)].

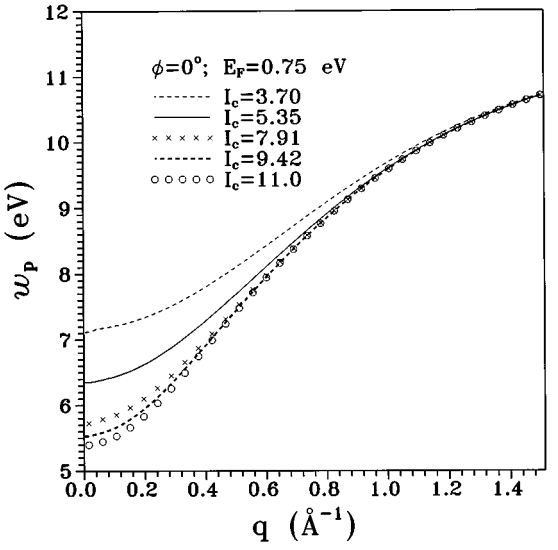

FIG. 10. Same plot as Fig. 9, but calculated at $\phi=0°$, $E_F=0.75$ eV, and various I_c.

Moreover, the interband excitations from the saddle points near the Q points, which is associated with the π plasmon, occur at the high-frequency range. Therefore, the vanishing ϵ_1 at the high-frequency range is hardly affected by the Fermi surface; i.e., the effect of E_F on the π-plasmon frequency would be negligible. In short, the enhanced interlayer distances should be an important influence in reducing the π-plasmon frequencies of the stage-1 graphite $FeCl_3$.[8]

The 2D rigid band could explain the measured π plasmons in the stage-1 AGIC's. It is further applied to calculate the π-plasmon frequencies of the stage-1 C_8M (DGIC's).[9] The π-plasmon characteristics of DGIC's are similar to those of AGIC's within the rigid-band model. C_8K, C_8Rb, and C_8Cs have the interlayer distances 5.35, 5.65, and 5.94 Å, respectively.[1] I_c's are close to one another and their π-plasmon frequencies, as stated above, would be also. This prediction is supported by the experimental measurements. Grunes and Ritsko[9] measured the EELS of C_8M, and obtained $w_p \sim 6.19-6.25$ eV at $q=0.1$ Å^{-1}. The measured results are consistent with the calculated results 6.37–6.44 eV [the light solid curve in Fig. 10(b)]. The 2D rigid-band model is suggested to be still available in C_8M. There are other similar suggestions.[35,36]

IV. CONCLUDING REMARKS

In this work, the π-electronic excitations in graphite and stage-1 GIC's are studied within the RPA. The 2D superlattice model is utilized to calculate the excitation spectra and the q- and ϕ-dependent π-plasmon frequencies. Generally speaking, the π plasmons in these two systems have similar characteristics. The calculated results could explain the experimental measurements on graphite[6] and stage-1 graphite $FeCl_3$ (AGIC's).[8] They are also consistent with the measured plasmon frequencies of C_8M,[9] which implies that the 2D rigid-band model is still available in these DGIC's.[35–36] Similar studies could be further extended to semi-infinite graphite,[34] the $\pi+\sigma$ electronic excitations, and other related systems (e.g., the layered boron nitride).[7]

The excitation properties directly reflect the π-band characteristics, the special symmetry, the strong wave-vector dependence, and the anisotropic behavior. The critical points in the energy-wave-vector space could induce the singular structures in the dielectric functions and are thus associated with the π-electronic collective excitations. The π plasmon has a strong dispersion relation with q, and at small q, it behaves as an optical plasmon in a 3D EGS. The anisotropic behavior at the plane is clear at large q. Moreover, the interlayer Coulomb interactions are found to be very important in supporting the π plasmons at very small q and enhancing the plasmon frequencies.

Graphite and GIC's have the common excitation properties as mentioned above. However, there are two principal differences between them. First, the excitation spectra of GIC's are richer. In addition to the interband e-h excitations and the π plasmon, GIC's could exhibit the intraband e-h excitations and the intraband plasmon. The intraband plasmon, with $w_p \sim 1$ eV, exists in GIC's owing to the high-density free carriers. Both the intraband plasmon and the π plasmon belong to optical plasmons, while their causes and certain characteristics differ greatly from each other. They are, respectively, derived from the intraband excitations of the Fermi surface states near the P' points (also including the P points at $\phi=30°$) and the interband excitations of the saddle points near the Q points. The intraband plasmon is quickly damped down with increasing q, while the π plasmon could exist at large q. Second, the π-plasmon frequency of the stage-1 GIC's is lower. The enhanced interlayer distances are an important influence in reducing w_p. On the other hand, the effect of free carriers on w_p is negligible, since the intraband excitation energies are much lower than w_p.

ACKNOWLEDGMENTS

One of us (M.F.L.) thanks K. W.-K. Shung for useful discussions. This work was supported in part by the National Science Council of Taiwan, Republic of China under Grants No. NSC 85-2112-M-009-020 and No. 86-2112-M-009-006.

[1] M. S. Dresselhaus, and G. Dresselhadus, Adv. Phys. **30**, 139 (1981); M. S. Dresselhaus, *Intercalation in Layered Materials* (Plenum, New York, 1987).
[2] S. Iijima, Nature **354**, 56 (1991).
[3] H. W. Kroto, J. R. Heath, S. C. O'Brien, R. F. Curl, and R. E. Smalley, Nature **318**, 162 (1985).
[4] D. Ugarte, Nature **359**, 707 (1992).
[5] E. A. Taft and H. R. Philipp, Phys. Rev. **138**, A197 (1965).
[6] K. Zeppenfeld, Z. Phys. **243**, 229 (1971); Opt. Commun. **1**, 119 (1969).
[7] U. Buchner, Phys. Status. Solidi B **81**, 227 (1977).
[8] J. J. Ritsko and M. J. Rice, Phys. Rev. Lett. **42**, 666 (1979).
[9] L. A. Grunes and J. J. Ritsko, Phys. Rev. B **28**, 3439 (1983); J. J. Ritsko; *ibid.* **25**, 6452 (1982).
[10] R. Kuzuo *et al.*, Jpn. J. Appl. Phys. **31**, L1484 (1992); V. P. Dravid *et al.*, Science **259**, 1601 (1993); P. M. Ajayan *et al.*, Phys. Rev. B **47**, 6859 (1993); L. A. Bursill *et al.*, *ibid.* **49**, 2882 (1994).
[11] G. Gensterblum, J. J. Pireaux, P. A. Thiry, R. Caudano, J. P. Vigneron, Ph. Lambin, and A. A. Lucas, Phys. Rev. Lett. **67**, 2171 (1991).
[12] A. A. Lucas, L. Henrard, and Ph. Lambin, Phys. Rev. B **49**, 2888 (1994).
[13] P. R. Wallace, Phys. Rev. **71**, 622 (1947).
[14] J. C. Slonczewski and P. R. Weiss, Phys. Rev. **109**, 272 (1958).
[15] F. Bassani and G. Pastori Parravicini, Nuovo Cimento **50**, 95 (1967).
[16] D. L. Greenaway, G. Herbeke, F. Bassani, and E. Tosatti, Phys. Rev. B **178**, 1340 (1969).
[17] G. S. Painter and D. E. Ellis, Phys. Rev. B **1**, 4747 (1970).
[18] M. Tsukada, K. Nakao, Y. Umeura, and S. Nagai, J. Phys. Soc. Jpn. **32**, 54 (1972).
[19] S. B. Trickey, F. Muller-Plathe, G. H. F. Diercksen, and J. C. Boettger, Phys. Rev. B **45**, 4460 (1992).
[20] J. Blinowski, Nguyen Hy Hau, C. Rigaux, J. P. Vieren, R. Le

Toullee, G. Furdin, A. Herold, and J. Melin, J. Phys. (Paris) **41**, 47 (1980).

[21] *Graphite Intercalation Compounds I*, edited by H. Zabel and S. Solin (Springer-Verlag, New York, 1990); *Gaphite Intercalation Compounds II*, edited by H. Zabel and S. Solin (Springer-Verlag, New York, 1992).

[22] R. C. Tatar, and S. Rabii, Phys. Rev. B **25**, 4126 (1982).

[23] J.-C. Charlier, J.-P. Michenaud, and X. Gonze, Phys. Rev. B **46**, 4531 (1992).

[24] E. T. Jesen, R. E. Palmer, W. Allison, and J. F. Annett, Phys. Rev. Lett. **66**, 492 (1991).

[25] D. Pines, and P. Nozieres, *The Theory Of Quantum Liquids* (Benjamin, New York, 1966).

[26] E. J. Mele and J. J. Ritsko, Solid State Commun. **33**, 937 (1980).

[27] K. W.-K. Shung, Phys. Rev. B **34**, 979 (1986); **34**, 1264 (1986); M. F. Lin and K. W.-K. Shung, *ibid.* **53**, 1109 (1996).

[28] J. W. McClure, Phys. Rev. B **104**, 666 (1956).

[29] H. Ehrenreich and M. H. Cohen, Phys. Rev. **115**, 786 (1959).

[30] N. D. Mermin, Phys. Rev. B **1**, 2362 (1970).

[31] S. Das Sarma and J. J. Quinn, Phys. Rev. B **25**, 7603 (1982); A. C. Teslis, and J. J. Quinn, *ibid*. **29**, 3318 (1984).

[32] L. Van Hove, Phys. Rev. **89**, 1189 (1953).

[33] M. F. Lin and K. W.-K. Shung, Phys. Rev. B **50**, 17 744 (1994).

[34] U. Diebold, A. Preisinger, P. Schattschneider, and P. Varga, Surf. Sci. **197**, 430 (1988).

[35] P. Alstrom, Synth. Met. **15**, 311 (1986).

[36] G. L. Doll, M. H. Yang, and P. C. Eklund, Phys. Rev. B **35**, 9790 (1987).